

Regular Article

Facile synthesis of carbon nanotubes covalently modified with ZnO nanorods for enhanced photodecomposition of dyes



Weiwei Tie^{a,b}, Zhao Zheng^{a,b}, Chao Xu^{a,b}, Zhi Zheng^{a,b}, Surjya Sarathi Bhattacharyya^d, Weiwei He^{a,b,*}, Seung Hee Lee^{c,*}

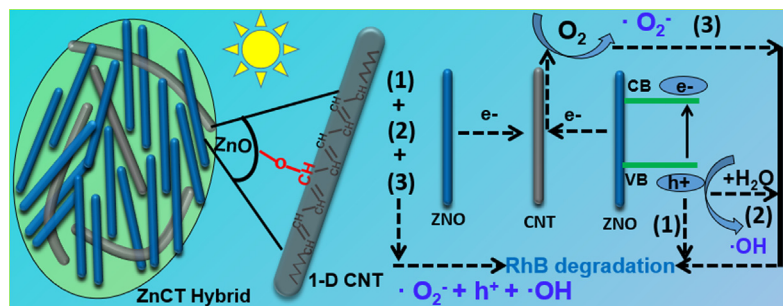
^aKey Laboratory of Micro-Nano Materials for Energy Storage and Conversion of Henan Province, School of Advanced Materials and Energy, Institute of Surface Micro and Nanomaterials, Xuchang University, Xuchang, Henan 461000, China

^bHenan Joint International Research Laboratory of Nanomaterials for Energy and Catalysis, Xuchang University, Xuchang, Henan 461000, China

^cApplied Materials Institute for BIN Convergence, Department of BIN Convergence Technology and Department of Polymer Nano-Science and Technology, Chonbuk National University, Jeonju, Jeonbuk 561-756, South Korea

^dAsutosh College, 92, Shyamaprasad Mukherjee Road, Kolkata 700 026, West Bengal, India

GRAPHICAL ABSTRACT



ARTICLE INFO

Article history:

Received 25 August 2018

Revised 12 November 2018

Accepted 12 November 2018

Available online 13 November 2018

Keywords:

Zinc oxide

Carbon nanotube

Anisotropic growth

Photocatalytic properties

Covalent bonding

ABSTRACT

Utilizing a one-pot solvothermal procedure novel one-dimensional zinc oxide–carbon nanotube nanohybrids (ZnCT) were synthesized in alcohol-alkali solution, free of catalytic assistance. The ZnCT hybrids were prepared through covalent modification of zinc oxide nanorods (ZnO NRs) with functionalized carbon nanotubes (f-CNTs). The morphology and microstructure of as-prepared ZnCT hybrids were characterized by scanning electron microscopy (SEM), powder X-ray diffraction, Raman, X-ray photoelectron and UV–vis absorption spectroscopies. SEM images of the ZnCT hybrids indicated that the ZnO_{ethanol} NRs grew longer along the vertical radial (0 0 0 1) surface and aggregated to a lesser extent than the analogous ZnO_{methanol} NRs. Photodegradation analysis showed that the off-white ZnCT_{ethanol} hybrid with ascendant UV–visible light absorption had displayed superior photocatalytic activity towards Rhodamine B (RhB) dyes than either pure ZnO_{ethanol}, ZnO_{methanol} NRs or ZnCT_{methanol} hybrid, among which the photocatalytic activity of ZnO_{ethanol} NRs was better than that of ZnO_{methanol} NRs. Raman and X-ray photoelectron spectroscopy analyses confirmed a strong interaction between f-CNTs and ZnO_{ethanol} NRs in ZnCT_{ethanol} hybrid, in which Zn ions were chemically bonded to negatively charged oxygen-containing groups at the graphene-like surface of f-CNTs. The enhanced separation lifetime of the photo-generated electron-hole observed by surface photovoltage and photocurrent measurements of the ZnCT_{ethanol} hybrid was attributed to the efficient covalent linking of Zn–O–C and close contact

* Corresponding authors at: Key Laboratory of Micro-Nano Materials for Energy Storage and Conversion of Henan Province, School of Advanced Materials and Energy, Institute of Surface Micro and Nanomaterials, Xuchang University, Xuchang, Henan 461000, China (W. He); Applied Materials Institute for BIN Convergence, Department of BIN Convergence Technology and Department of Polymer Nano-Science and Technology, Chonbuk National University, Jeonju, Jeonbuk 561-756, South Korea (S. H. Lee).

E-mail addresses: tieweiwei@xcu.edu.cn (W. Tie), heww1982@163.com (W. He), lsh1@chonbuk.ac.kr (S.H. Lee).

configuration between the f-CNTs and ZnO_{ethanol} NRs. Further controlled photodegradation and electron spin resonance (ESR) analyses revealed that the photodegradation of RhB dyes resulted from photogenerated holes, and radical species, such as $\cdot\text{O}^{2-}$, $\cdot\text{OH}^-$, which were formed *in-situ*. Details of the photocatalytic mechanism were also explored herein.

© 2018 Elsevier Inc. All rights reserved.

1. Introduction

Interest in the development of zinc oxide (ZnO) semiconductors with distinctive morphologies and sizes for the complete elimination of toxic chemicals released to environment is attributed to their attractive performance, such as strong oxidation capability and environmental friendliness [1–3]. However, ZnO nanocrystals, which exemplify a wide band gap semiconductor material, exhibit a negative photo response of visible light, such as inefficient absorption of visible light and rapid recombination of photogenerated charge carriers [4,5]. More importantly, strong van der Waals interaction between individual ZnO nanocrystals always results in the formation of clusters or aggregates, which nullifies their catalytic properties and consequently limits their large-scale practical applications [6,7]. To improve the practical applicability of ZnO nanocrystals for pro-environmental applications, it is therefore necessary to develop an optimal structure-performance photocatalyst with excellent photodecomposition activity driven by sunlight rather than ultraviolet light so as to be photoactive at a wide wavelength range and can absorb sunlight efficiently.

ZnO nanocrystals possessing one-dimensional (1-D) morphology have attracted considerable interest due to their pronounced morphological effect in nanoscale optoelectronic devices and photocatalytic applications [8,9]. Recently, a single-step, large-scale hydrothermal method was successfully developed for the synthesis of small diametric 1-D ZnO nanorods (ZnO NRs) with different aspect ratios [10]; however, few works have been done to explore the reaction solvent-induced morphological effect on their photocatalytic activity. Consequently, this work aims to efficiently improve the photocatalytic performance of 1-D ZnO NRs by modulating their light absorption and electron-hole photo-recombination properties. Recent advancements in the functionalization of 1-D ZnO NRs with carbonaceous nanomaterials have facilitated the design and development of novel photocatalytic nanohybrids [11–15]. As the prototypical 1-D carbon material platform, carbon nanotubes (CNTs) can not only increase the efficiency of wideband sunlight absorption and electronic excitation from 1-D ZnO NRs due to their high surface area and the black optical absorption, but also facilitate rapid transit of the photogenerated electrons from ZnO to the conductive graphene surface of CNTs because of its high charge carrier mobility and excellent electron conductivity [16,17]. These advantages efficiently prolong the separation time of the photogenerated electron-hole pairs and consequently the photodegradation capability of the target ZnO-CNT hybrid [18,19]. Furthermore, 1-D CNTs could function as an effective conductive spacer to prevent the aggregation of ZnO NRs than other two-dimensional carbonaceous nanomaterials (i.e. graphene or graphene oxide) due to a better shape matching between the 1-D CNTs and ZnO NRs than between 2-D materials and ZnO NRs [7,20–25].

Motivated by the above analysis, the work presented herein adopts a simple one-pot solvothermal method without addition of dispersants to afford novel ZnO-CNT nanohybrids (ZnCT). The as-prepared ZnCT hybrids consist of dispersive 1-D CNTs covalently linked to 1-D ZnO NRs through direct interatomic bonding (Zn–C or Zn–O–C). It should be noted that the main reason why we have chosen 1-D CNT to modify ZnO nanorods is because it

not only acts as conductive carriers for the acceleration of electron transfer and to improve light-harvesting efficiency, but also acts as spacers for the prevention of aggregation of the 1-D ZnO NRs. The similarity of the structural features of the 1-D CNTs and the ZnO NRs provide a better match for the prevention of aggregation than would be expected in the case of 2-D graphene [7,22,23]. The as-prepared ZnCT_{ethanol} composite is photocatalytically active, as evidenced by the near-complete degradation of 1 mg/mL Rhodamine B (RhB) dye by only 10 mg of the composite. The photocatalytic activity of this material is attributed to the covalent linking and contact matching interaction of the dispersive CNTs with the ZnO NRs, which accelerate the separation of photogenerated electron-holes and extend the light absorption range and intensity. Furthermore, mechanistic study of this hybrid material suggests that the formation of photogenerated holes and generation of other reactive radical species such as $\cdot\text{O}^{2-}$ and $\cdot\text{OH}^-$ are responsible for the photodegradation of organic dyes.

2. Experimental

2.1. Materials

Carbon nanotubes (Length: 10–30 μm ; OD: 20–30 nm; purity: >95%) used for preparing ZnCT hybrids were supplied by the Chengdu Organic Chemicals Co. Ltd. Anhydrous zinc acetate (ZnAc₂, 99.5%) was obtained from Aladdin Co. Ltd. H₂SO₄ (98%), HNO₃ (60%), sodiumhydroxide (NaOH), Rhodamine B (RhB), anhydrous ethanol and methanol were obtained from China Reagent Company, LTD. All the chemicals were purchased and directly used as analytical grade without further treatment. The carbon nanotubes were functionalized following an acid oxidation process modified from a previously reported procedure [6]. The fabrication details are described as follows: MWCNT powder (100 mg) was combined with a 3:1 (v/v) mixture (50 mL) of HNO₃ (68%) and H₂SO₄ (98%) in a reactor and kept stirring at 50 °C for 8 h. Following centrifugation at 12000 rpm for 30 min, the supernatant was decanted and filtered through a 0.2 μm anodic alumina membrane (Whatman). The solution was subjected to centrifugation and wash cycled using deionized water until a neutral pH was obtained. Drying the resultant solution in a vacuum oven at 60 °C gave rise to power product, hereafter referred to as f-CNT.

2.2. Preparation of ZnCT hybrids

In a typical procedure, f-CNT (2 mg) was sonicated for 30 min in ethanol or methanol (10 mL) to obtain a homogeneous dispersion. Ethanol or methanol (20 mL), solution of anhydrous zinc acetate (0.1832 g) and sodiumhydroxide (0.4015 g) were added to the above mentioned solution while stirring. The homogeneous solution was then maintained at 150 °C for 24 h in an autoclave. The prepared ZnCT composite was isolated after washing with distilled water and ethanol several times and drying under vacuum at 40 °C for 12 h. The prepared samples were denoted ZnCT_{ethanol} or ZnCT_{methanol}, based on the solvent that was used for their preparation. For comparison, pure ZnO_{ethanol} and ZnO_{methanol} were prepared following the same procedure without the addition of the f-CNTs.

2.3. Characterization

Surface morphology of the ZnCT hybrid was observed using a scanning electron microscope (SEM, Nova NanoSEM 450, FEI Company, USA). The crystalline phase was determined by analyzing X-ray diffraction profile collected on a Bruker D8 Advance diffractometer equipped with Cu K α sealed-tube radiation ($\lambda = 1.5406 \text{ \AA}$). Raman spectroscopic analysis was carried out using a Renishaw inVia Raman spectrometer with a laser excitation of 532 nm. X-ray photoelectron spectroscopic analysis was executed out using a XPS spectrometer (Thermo escalab 250XI, USA) with Al K α radiation ($h\nu = 1486.6 \text{ eV}$). UV–vis spectra were recorded using a UV–Vis–Infrared spectrophotometer (Agilent Cary-5000). Electron-spin-resonance analysis (ESR) was performed utilizing a Bruker A300 spectrometer working with an X-band frequency of 9.845 GHz.

Transient surface photovoltage (TPV) analysis was carried out following the method prescribed by Lei et al. [26]. Powder samples of almost 2 mg for ZnO_{ethanol} and ZnCT_{ethanol} were loaded onto an indium tin oxide (ITO) coated glass substrate and covered with a second ITO coated glass substrate. Mica spacers were used to maintain the suitable gap between the two electrodes. The third-harmonic Nd: YAG laser (Quantel Brilliant Eazy: BRILEZ/IR-10) had been utilized to supply laser pulses (355 nm with a pulse width of 4 ns), and TPV signals were recorded using a digital oscilloscope with frequency of 500 MHz (TDS 3054C, Tektronix).

Photocurrent measurements performed on a CHI 660 potentiostat (CH Instruments) were carried out under simulated sunlight irradiation with a power of ca. 100 mW/cm² using a standard three-electrode system immersed in a 0.1 M KCl solution [27]. To prepare a working electrode for the photocurrent measurements, the ZnCT_{ethanol} composites or pure ZnO_{ethanol} NRs (6 mg) were first dispersed in ethanol (1 mL) via sonication for 15 min, respectively; the resultant suspension was then dropped onto ITO glass and dried for 2 h at 60 °C. Platinum foil electrode and Ag/AgCl electrode were used as the counter electrode and reference electrode, respectively.

2.4. Photocatalytic activity

The photocatalytic activity of the prepared photocatalysts was probed via addition of the composites to an aqueous solution of powdered RhB dye under stimulating sunlight (Xe light, 500 W). Evaluation equation of photocatalytic activity (κ) is described as follows: $\kappa = C_0/C_t$ [8,12,27], where C_0 and C_t are the initial concentration and concentration at sunlight irradiation time (t) of RhB dye. Powdered photocatalysts (10 mg) were dispersed in an aqueous solution of RhB (20 mg/L, 50 mL) via 1 min of ultrasonication. Prior to irradiation with sunlight, the aqueous mixture of powdered RhB dyes and photocatalyst was magnetically stirred in the dark for 40 min to ensure surface adsorption equilibrium of RhB dye on composites. The suspension was irradiated and subjected to UV–vis analysis after regular intervals of irradiation. After centrifugation, the concentration of unreacted RhB in solution was quantified using the characteristic absorption band observed at 554 nm in the UV/vis spectra. The photocatalytic activities of the photogenerated active species of hydroxyl radicals ($\cdot\text{OH}^-$), superoxide radicals ($\cdot\text{O}^{2-}$), holes (h^+) and electrons (e^-) were determined by using 1.0 mM *t*-butanol (a quencher of $\cdot\text{OH}^-$), 1.0 mM *p*-benzoquinone (benzoquinone, a quencher of $\cdot\text{O}^{2-}$), and 1.0 mM methanol (a quencher of h^+), and 1.0 mM hydrogen peroxide (a quencher of e^-), respectively. This measurement was conducted following a similar protocol to previously reported tests for photocatalytic activity [12,27].

3. Result and discussion

As described above, preparation of the ZnCT_{methanol} and ZnCT_{ethanol} hybrids is prepared via addition of anhydrous zinc acetate and sodium hydroxide to a homogeneous dispersion of f-CNTs in methanol or ethanol, followed by heating at 150 °C for 24 h. We have investigated the ZnCT_{methanol} and ZnCT_{ethanol} hybrids under SEM to directly observe the surface morphologies and to explore the influence of solvent effects on their morphologies. The SEM micrographs shown in Fig. 1 indicate dissimilar rod morphologies between the two hybrids. SEM analysis of the ZnCT_{methanol} hybrid (Fig. 1(a–c)) clearly exhibits a significant aggregation of the ZnO NRs with nanorods measuring about ~ 0.5 – $1.0 \mu\text{m}$ in length and about 20 nm in width; moreover, contact between individual ZnO NRs is closer than the contact between ZnO NRs and the CNTs.

Conversely, analysis of the ZnCT_{ethanol} hybrid (Fig. 1(d–f)) displays a uniform rod dispersal of the ZnO NRs and CNTs with the similar rod shape with about 30 nm in width and about 1–5 μm in length, where the length of ZnO NRs is ten times that measured for the ZnCT_{methanol} hybrid, and a stronger interaction between the CNTs and ZnO NRs is observed. The close ZnO NR–CNT contact in the ZnCT_{ethanol} hybrid suggests that the CNTs can act as a spacer between ZnO NRs to inhibit their further aggregation.

The controllable anisotropic growth process of rod-like ZnCT hybrid during solvothermal processes has been previously demonstrated in the literature [10]. Electrostatic forces are averaged to afford chemical absorption of Zn²⁺ ions onto the negatively charged graphene-like surfaces of CNTs. Following absorption of the positively changed zinc ions, nucleation of ZnO on the graphene-like surfaces of CNTs is facilitated through intermolecular hydrogen bonding and electrostatic attraction between ZnO²⁻ and the functionalized containing oxygen groups on the CNTs [2]. Generally, the growth rate of the ZnO nucleation sites is dependent on the specific crystallization conditions (i.e. supersaturation, temperature, solvents and impurities) [8]. As the Zn terminated (00 $\bar{1}$) planes and the symmetry-related (00 $\bar{1}$) planes in polar ZnO crystal are active, the preferential growth of the (001) and (00 $\bar{1}$) planes along the *c* axis is observed [8,9]. Due to the higher polarity of methanol relative to ethanol due to distinct chain length of alcohols, a stronger interaction is predicted between methanol and the polar crystal plane of ZnO [8]. Consequently, we expect to see a difference in the crystal growth pattern of polar ZnO NRs as a manifestation of the crystal interface-solvent interactions. Applying the one-pot solvothermal synthetic procedure described in this work, different sized 1-D ZnO NRs are indeed obtained in different solvent mediums. This result clearly indicates the morphologies of ZnO NRs can be successfully controlled through the variety of solvent, and further effectively moderate van der Waals-induced aggregation tendency of ZnO NRs.

To compare the structure and phase between the ZnCT_{ethanol} hybrid and pure ZnO_{ethanol} or ZnO_{methanol}, the X-ray diffraction (XRD) patterns are collected. As shown in Fig. 2, the XRD patterns collected for pure ZnO_{ethanol}, ZnO_{methanol}, ZnCT_{methanol} and ZnCT_{ethanol} hybrids all exhibit diffraction peaks at $2\theta = 31.78^\circ$, 34.48° , 36.31° , 47.61° , 56.66° , 62.94° , 66.64° , and 68.00° pertaining to the (100), (002), (101), (102), (110), (103), (200), (112), and (201) planes of ZnO, respectively; the observed diffraction peaks are consistent with hexagonal phase wurtzite ZnO (JCPDS No. 36–1451) [10]. However, the (002) diffraction peaks at 34.48° for ZnO_{methanol} and ZnCT_{methanol} are more intense than those observed for either ZnO_{ethanol} and ZnCT_{ethanol}; while the (100)/(002) ratios are approximately 0.92 and 0.89 for ZnO_{methanol} and ZnCT_{methanol}, whereas the height of the (002) diffraction peak decreases significantly and then the (100)/(002) ratio increases to 1.39 and 1.05 for ZnO_{ethanol} and the ZnCT_{ethanol}

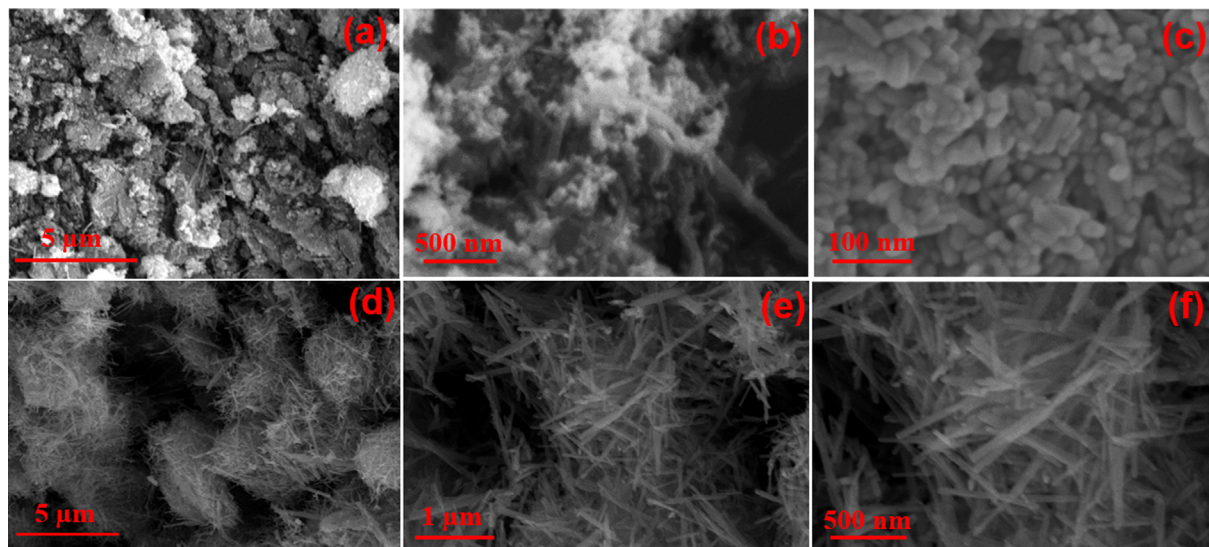


Fig. 1. Scanning electron micrograph of ZnCT_{methanol} (a, b, c) and ZnCT_{ethanol} hybrid (d, e, f) hybrid.

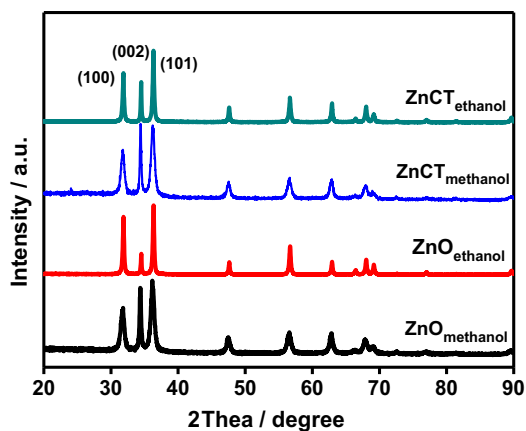


Fig. 2. XRD spectra of ZnO_{ethanol}, ZnO_{methanol}, ZnCT_{methanol} and ZnCT_{ethanol} hybrid.

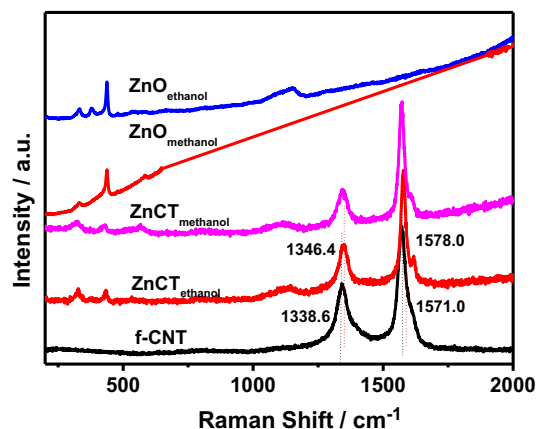


Fig. 3. Raman spectra of ZnO_{ethanol}, ZnO_{methanol}, ZnCT_{methanol} and ZnCT_{ethanol} hybrid.

hybrid, respectively. The differences observed in the relative intensity ratio of the (1 0 0) and (0 0 2) peaks in the XRD patterns of these materials suggest that the preferential growth of ZnO NRs along the c axis can be controlled through careful selection of reaction solvent. The lack of a separate peak corresponding to CNTs in the ZnCT_{ethanol} hybrids is probably attributed to the low intensity and loading content of CNTs [28]. Additionally, the peaks of ZnO NRs in ZnCT_{methanol} appear to be diffused in comparison with ZnO_{ethanol} NRs in ZnCT_{ethanol}, which indicates smaller particle size for ZnCT_{methanol}. One can estimate particle size using Scherrer equation: $\tau = k\lambda/\beta\cos\theta$, where τ is the mean size of the ordered (crystalline) domains, which may be equal to or smaller than the grain size, 'k' is a dimensionless shape factor, with a value close to unity, ' λ ' is X-Ray wavelength, ' β ' is the line broadening at half of the maximum intensity, and ' θ ' is the Bragg angle [4]. The averaged sizes of the ZnO NRs in ZnCT calculated using the value obtained from the most intense peak are approximately 12.4 nm for ZnO_{methanol} NRs in ZnCT_{methanol} and 27.7 nm for ZnO_{ethanol} NRs in ZnCT_{ethanol} samples. The results successfully confirm the synthesis of ZnO NRs utilizing a facile solvothermal process, which are further consistent with the distinct rod shape displayed in SEM measurements.

The introduction of f-CNTs into the ZnCT hybrid is confirmed by comparison of the Raman spectra obtained for pure ZnO_{ethanol}, pure

ZnO_{methanol}, f-CNTs, ZnCT_{methanol} and ZnCT_{ethanol}, depicted in Fig. 3. The spectrum for pure ZnO_{ethanol} displays three characteristic Raman bands at 329 ($E_2^{\text{high}} - E_2^{\text{low}}$ mode), 375 ($A_1^1(\text{TO})$ mode), and 438 cm^{-1} (E_2^{high} mode) [14]. Only two Raman bands at $\sim 329 \text{ cm}^{-1}$ and $\sim 435 \text{ cm}^{-1}$ are observed in this region of the spectrum of the pure ZnO_{methanol}, ZnCT_{methanol} and ZnCT_{ethanol} hybrid, corresponding to the $E_2^{\text{high}} - E_2^{\text{low}}$ mode and E_2^{high} mode for pure ZnO NRs. In general, Raman peak around 375 cm^{-1} results from the polar $A_1^1(\text{TO})$ mode, indicating that there is a change in lattice constants [28,29]. From our previous investigation in Fig. 2, it is observed the (1 0 0)/(0 0 2) ratio of diffraction peaks is approximately 0.92 for ZnO_{methanol}, however, in which this ratio increases to 1.39 for ZnO_{ethanol} due to significant decrease of the intensity of the (0 0 2) diffraction peak. Additionally, the peak of ZnO NRs appears to be diffused in comparison with ZnO_{ethanol} NRs, which displays similar situation in that of ZnCT_{methanol} and ZnCT_{ethanol}, which indicates smaller particle size for ZnO_{methanol} NRs compared to ZnO_{ethanol} NRs. These different (1 0 0)/(0 0 2) ratios and different crystal sizes clearly point out distinct crystal growth of ZnO NRs along the c axis for ZnO_{ethanol} and ZnO_{methanol}. Therefore, the disappearance of the $A_1^1(\text{TO})$ mode at 375 cm^{-1} for ZnO_{methanol} compared to that of ZnO_{ethanol}, has clearly reflected the strength variety of the polar lattice bonds due to the different polar $A_1^1(\text{TO})$ mode.

Additionally, the other representative peaks observed in Raman spectra of ZnO are found to be less intense, suggesting that the hybrid form of ZnO is highly crystalline with a hexagonal wurtzite phase [14]. Note that this ZnCT_{ethanol} system with in-situ reaction obtained ZnO NRs in ethanol medium has been focused herein due to its photolysis superiority displayed onto RhB dyes in the following paragraphs. Comparison of the spectra for f-CNTs and ZnCT_{ethanol} hybrid reveals a distinct G-band around 1575 cm⁻¹ (1571 cm⁻¹ for f-CNTs and 1578 cm⁻¹ for ZnCT_{ethanol}), which is attributed to the E_{2g} vibrational mode of the sp² bonded carbon and a D-band around 1340 cm⁻¹ (1338 cm⁻¹ for f-CNTs and 1346 cm⁻¹ for ZnCT_{ethanol}), which is attributed to the A_{1g} mode breathing vibrations of the six-membered sp² carbon rings. The G band shifting from 1571 cm⁻¹ to 1578 cm⁻¹ in the ZnCT_{ethanol} hybrid as compared to the f-CNTs is indicative of a distinct charge transfer between the graphitic structures and the carboxyl and hydroxide related oxygen functional groups or ZnO NRs [4,29]. Additionally, the ratio of D- to G-band intensity (I_D/I_G) for the ZnCT_{ethanol} hybrid (0.54) is higher than the ratio calculated for f-CNTs (0.43), which may be attributed to an increase in number of small sp² domains during the ZnCT_{ethanol} hybrid [4,14]. These results indicate that the functionalization and incorporation of ZnO NRs with f-CNT have been successfully realized and have little effect on the crystalline size of the ZnCT_{ethanol} hybrid.

A comparison of light absorption by ZnO_{ethanol} and the ZnCT_{ethanol} hybrid is afforded via analysis of UV-vis absorption spectra, as depicted in Fig. 4. The spectrum for pure ZnO_{ethanol} exhibits a significant UV absorption band at 367 nm, corresponding to the free excitonic absorption of ZnO particles [28], and relatively weak visible light absorption that is attributed either to defects induced chemical interactions in ZnO, or to the band gap reduction effect of ZnO, or to a combination of both of these two effects [4]. Similar to the spectrum of pure ZnO_{ethanol}, the ZnCT_{ethanol} hybrid also displays a sharp absorption in the UV region, and cumulatively broad and intense background absorption across the whole visible region, which is not observed with pure ZnO. Therefore, the increase of optical absorption across the entire visible (400–800 nm) range suggests the successful incorporation of ZnO NRs with the CNTs in the formation of the ZnCT_{ethanol} hybrid, which indicates that introduction of f-CNTs intensifies the absorbance of visible light by ZnO NRs. This increased capacity for visible light absorbance may result from one or more of the following reasons: (1) the passivation of the CNT surface upon the growth of rod-shaped ZnO NRs, (2) the introduction of defects to the ZnO matrix through chemical interactions, or (3) the reduction of the band gaps of ZnO, which facilitates the absorption of longer-wavelength light [14].

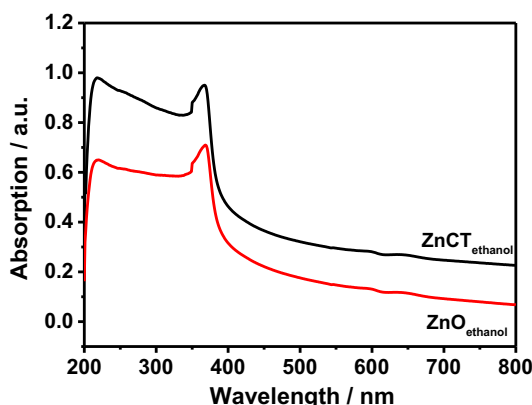


Fig. 4. UV-vis absorption spectra of ZnO_{ethanol} NRs and ZnCT_{ethanol} hybrid.

Chemical composition and bonding properties of the f-CNT-hybridized ZnO_{ethanol} NRs are further investigated by XPS analysis. The Zn core-level XPS spectrum of pure ZnO_{ethanol} NRs shows two symmetric peaks centered at 1021.1 and 1044.4 eV, as shown in Fig. 5, which are assigned to the Zn 2p_{3/2} and Zn 3p_{1/2} spin-orbital splitting photoelectrons, respectively [30]. In the Zn 2p spectrum of the ZnCT_{ethanol} hybrid, the peak position centers are located at 1022.6 eV and 1045.5 eV. The shift in peak position relative to the pure ZnO_{ethanol} NRs indicates a new chemical bond between the ZnO_{ethanol} and the f-CNTs. To further probe the chemical bonding between ZnO NRs and f-CNTs in the ZnCT_{ethanol} hybrid, high resolution O 1s core level spectra of the ZnCT_{ethanol} hybrid is obtained, which is analyzed using a peak fitting program to deconvolute the overlapping peaks (Fig. 6). As shown in Fig. 6, the deconvoluted O 1s peak consists of several components, which are located at 530.88, 531.58, 532.28, 533.28 and 534.18 eV, respectively. Normally, the O 1s in XPS spectra displays three kinds of chemical states, which are attributed to crystal lattice oxygen, chemically bonded oxygen and physically adsorbed oxygen with an increase in binding energy, respectively [31–33]. The peaks at 530.88 and 531.58 eV correspond to the O²⁻ from the wurtzite structure of the ZnO lattice and the O²⁻ in the oxygen deficient region of the ZnO matrix, respectively [34]. The blue-shifting of the 531.58 eV peak relative to that at 530.88 eV suggests a Zn-C interaction, affected by the large difference in electronegativity of Zn and C. The binding energies of the peaks located at 532.28 and 533.28 eV could be slightly higher than that for the 531.58 eV peak due to the more electronegative oxygen environment [14,35]. Therefore, the peaks at 532.28 and 533.28 eV could be recognized due to the chemical bonding of the C=O and C–O functional groups linking to Zn at the poorly crystalline carbons of graphene, respectively [36], which indicates that C may be directly chemically bonded to Zn using Zn–C, or indirectly bonded to Zn using –O–Zn–C via the oxygens in C–O or C=O of graphene in the ZnCT_{ethanol} composite. Due to their higher binding energy the component at 534.18 eV should originate from physically adsorbed oxygen in carboxylic groups or surface functional hydroxy groups in water molecules with increased binding energy [31–33]. The analysis of the de-convoluted peaks shown in the O 1s core level spectrum is a powerful evidence to support the existence of chemical bonding between Zn and C in the ZnCT_{ethanol} hybrid.

The charge separation and transfer capacities of a photocatalyst are an indicator of its photocatalytic efficiency. Surface transient photovoltage analysis (TPV) is carried out to measure the photo-induced charge carrier dynamics of pure ZnO_{ethanol} NRs and the prepared ZnCT_{ethanol} hybrid, specifically probing the lifetime and transfer processes of the electron-hole pairs. The TPV measurement

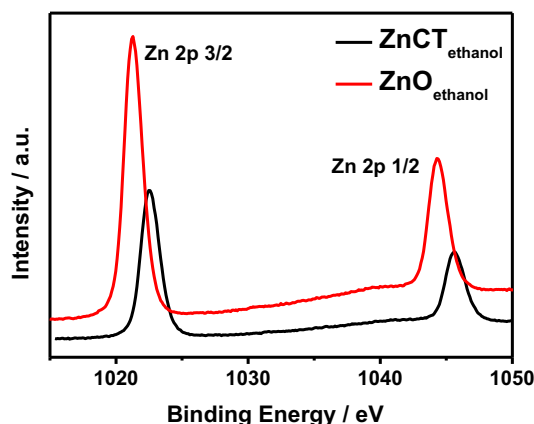


Fig. 5. XPS spectra of Zn 2p spectra of ZnO_{ethanol} NRs and ZnCT_{ethanol} hybrid.

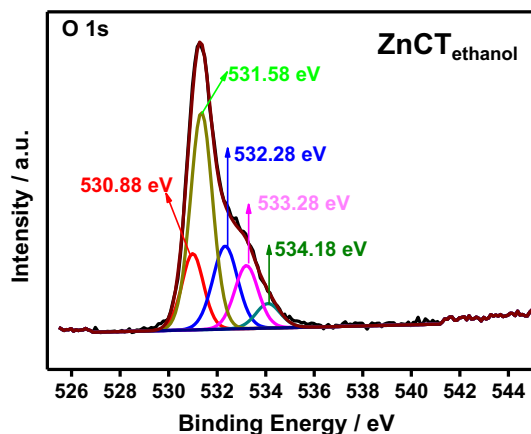


Fig. 6. XPS spectra of the O 1s core level of the ZnCT_{ethanol} hybrid.

said in elucidating the photocatalytic mechanism in the current system. Fig. 7 shows the measured TPV curves of pure ZnO_{ethanol} NRs and the ZnCT_{ethanol} hybrid, which displays distinct dynamic response process of a photo-generated carrier. The pure ZnO_{ethanol} NRs exhibit very short carrier separation process, while the ZnCT_{ethanol} hybrid has a relatively fast separation ratio and a long lifetime of photo-induced charge carrier. The lifetime of the photo-induced electron-hole pairs in pure ZnO_{ethanol} NRs is about 2×10^{-3} s, while a much longer lifetime is detected for the ZnCT_{ethanol} hybrid (10^{-2} s), suggesting a large separation of the photogenerated electrons and holes and also an efficient transfer of the photogenerated electrons to the graphene-like sheets of CNTs occurred in the ZnCT_{ethanol} hybrid [26]; moreover, the long lifetime of the electron-hole pair indicates that electron-hole pair recombination is quenched in the ZnCT_{ethanol} composite. The electron generation capacity of this material suggests a potential for applications in pollutant degradation, which will be discussed in the following paragraphs.

In order to further assess the photo-induced charge separation efficiency of the nanocomposite, the photocurrent is measured under on-off cycles of 100 mW/cm^2 sunlight source. The working electrodes are made by drop casting ($100 \mu\text{L}$, 1 mg/mL) on to an ITO electrode (1 cm^2) [37]. Fig. 8 shows the photocurrent measurements of ZnO_{ethanol} and ZnCT_{ethanol} for every On-Off cycle. The experimental current measured in this photoelectrochemical system reflects the generation of the available photoexcited electrons from these photocatalysts. From the photocurrent responses it is evident that the ZnCT_{ethanol} hybrid produces the maximum photocurrent, confirming larger separation of the electron-hole pairs

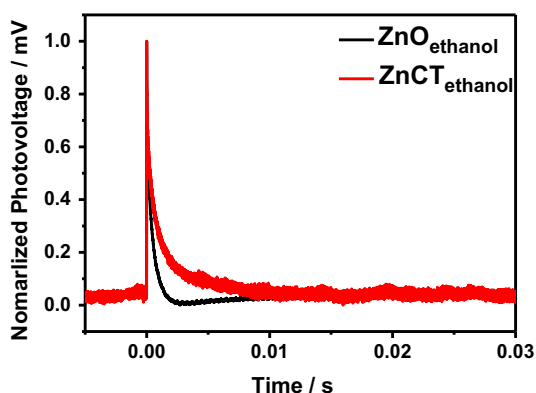


Fig. 7. Surface photovoltage spectra of ZnO_{ethanol} NRs and ZnCT_{ethanol} hybrid.

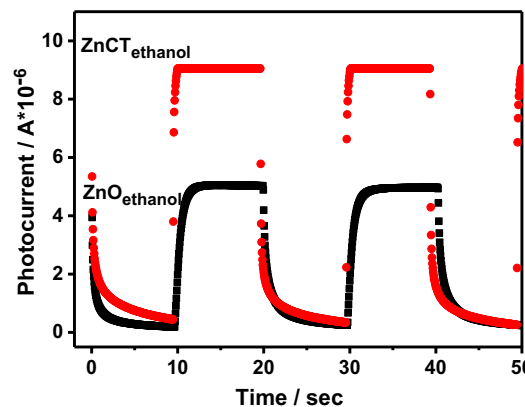


Fig. 8. The photocurrent response of ZnO_{ethanol} NRs and ZnCT_{ethanol} hybrid.

and transport of the electrons relative to pure ZnO_{ethanol} NRs tested. Specifically, the ZnCT_{ethanol} hybrid modified electrode exhibits a photocurrent two times higher than that of bare ZnO_{ethanol}. The increase of current intensity of the hybrid confirms efficient electron transfer through better 1-D shape matching between ZnO_{ethanol} NRs and CNTs extending the electron-hole lifetime of ZnCT_{ethanol} hybrid, which is consequently available for the photocatalytic degradation process as demonstrated in the enhanced photocatalytic degradation of RhB by the ZnCT_{ethanol} hybrid, which will be discussed in the following paragraphs. The photocurrent response is in agreement with previous discuss from the TPV measurements.

The photocatalytic degradation activity of pure ZnO_{methanol}, pure ZnO_{ethanol}, ZnCT_{methanol} and ZnCT_{ethanol} hybrid is demonstrated through the decomposition of a highly concentrated (0.02 mg/mL) aqueous solution of RhB dye. Sample solutions are exposed to solar-wave light radiation to initiate the photocatalytic process; the remaining, non-degraded dye is then measured using UV-Vis spectrometry. Fig. 9 shows that following 2 h of irradiation, 90.0% or 81% degradation of the RhB dye in the presence of the ZnCT_{ethanol} or ZnCT_{methanol} composite is observed, whereas only 74.0% and 55.0% degradation are achieved with pure ZnO_{ethanol} and ZnO_{methanol}, respectively. The results of this study demonstrate that pure ZnO_{ethanol} NRs have better photocatalytic degradation activity than that of ZnO_{methanol} NRs, and their photocatalytic degradation activity has been effectively enhanced through an introduction of CNTs into ZnO NRs for ZnCT_{methanol} and ZnCT_{ethanol} hybrids; however, the best catalytic activity is observed for the ZnCT_{ethanol} hybrid, which shows enhanced activity across the solar

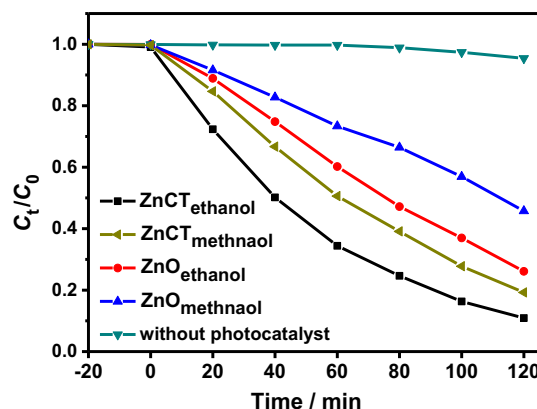


Fig. 9. Photocatalytic degradation under solar irradiation of RhB over ZnO_{methanol}, ZnO_{ethanol}, ZnCT_{methanol} and ZnCT_{ethanol} hybrid.

spectrum compared to pure $\text{ZnO}_{\text{ethanol}}$, $\text{ZnO}_{\text{methanol}}$ and $\text{ZnCT}_{\text{methanol}}$ hybrid. After completion of the degradation reaction, the $\text{ZnCT}_{\text{ethanol}}$ hybrid is recovered by centrifugation, washing, and drying. The catalyst is recycled up to 3 times prior to any loss of degradation activity, where activity is reduced to 90.0% after 3 cycles of the photocatalysis reaction. The recyclability of the catalyst indicates that the $\text{ZnCT}_{\text{ethanol}}$ photocatalyst is highly resistant to photo-corrosion. The efficient photocatalytic activity and recyclability of the $\text{ZnCT}_{\text{ethanol}}$ photocatalyst suggest a potential of this photocatalyst for practical applications.

To determine the specific oxidation pathway of RhB in the presence of the $\text{ZnCT}_{\text{ethanol}}$ hybrid, controlled photodecomposition experiments are carried out in an analogous fashion to the experiments described above, but in the presence of scavengers (Fig. 10). Different classes of scavengers are dropped into the RhB solutions to aid in mechanistic elucidation: a hole scavenger (methanol), a superoxide radical scavenger (benzoquinone), a hydroxyl radical scavenger (*t*-butanol), and e^- -trapping agents (hydrogen peroxide). The results of these experiments are highlighted in Fig. 10. Decomposition of the majority of the RhB dye (81%) still occurs in the presence of an e^- trapping agent (hydrogen peroxide), while only 30%–40% of RhB is decomposed when $\cdot\text{OH}^-$, h^+ , or $\cdot\text{O}_2^-$ radical trapping agents (*t*-butanol, methanol, benzoquinone) are introduced. Thus, the addition of methanol, *t*-butanol, or benzoquinone, to some extent, decrease the photodegradation efficiency of the $\text{ZnCT}_{\text{ethanol}}$ hybrid towards RhB dyes. Verification of the identity of the photo-induced reactive radicals as reactive oxygen species was attempted using an electron spin resonance (ESR) spin-trap technique (with 5,5-dimethyl-1-pyrroline N-oxide, DMPO or 2,2,6,6-Tetramethylpiperidine-1-oxyl, TEMPO). As shown in Fig. 11, three signals of TEMPO h^+ , DMPO- $\cdot\text{OH}$, and DMPO- $\cdot\text{O}_2^-$ are detected in the $\text{ZnCT}_{\text{ethanol}}$ suspension following irradiation with sunlight, which demonstrates that hole, hydroxyl, and superoxide radicals are involved in the photocatalysis process. Therefore, the results of this ESR experiment indicates that a synergistic effect of the reactive species of $\cdot\text{O}_2^-$ and $\cdot\text{OH}^-$, as well as h^+ radicals contributes to the photodegradation activity of $\text{ZnCT}_{\text{ethanol}}$ hybrid onto RhB dyes.

Consistent with above discussion, the photocatalytic oxidation mechanism of RhB by the $\text{ZnCT}_{\text{ethanol}}$ hybrid should follow the mixed oxidation pathway of hole (h^+), superoxide radical ($\cdot\text{O}_2^-$), and hydroxyl radical ($\cdot\text{OH}^-$) depicted in Fig. 12. The proposed mechanism for the photolysis of RhB is divided into three pathways: electrons and holes are generated by excitation of ZnO NRs or dye molecules (Path (1)); hydroxyl radicals are generated from the reaction of holes with H_2O (Path (2)); superoxide radicals are generated from the reaction of the corresponding electrons with dissolved O_2 (Path (3)). The generated massive reactive oxygen species (ROs) subsequently oxidize the RhB compounds [30,34].

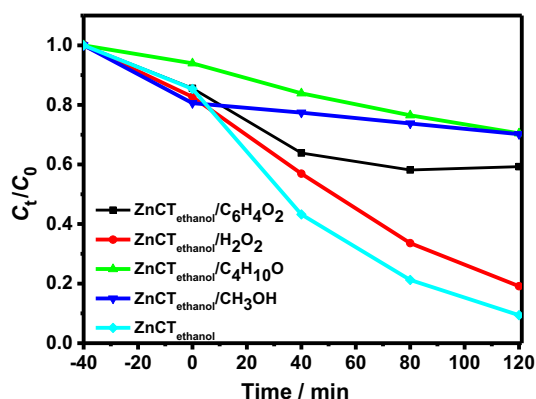


Fig. 10. Photodegradation dynamics of RhB in the presence of $\text{ZnCT}_{\text{ethanol}}$ with and without addition of *t*-butanol, methanol, benzoquinone, and hydrogen peroxide.

In this work, excitation of both ZnO NRs and RhB molecules should be involved in the photocatalytic degradation of RhB pollutant by the $\text{ZnCT}_{\text{ethanol}}$ hybrid under sunlight irradiation. First, solar light irradiation leads to the excitation of ZnO NRs or dye molecules and induces the generation of electrons. Then, rapid electron transfer will occur from the excited dyes (dye^*) directly to CNTs or indirectly from the conduction band of ZnO to CNTs, aided by the covalent bonding between the ZnO NRs and the CNTs [4,34]. Holes will be naturally generated accompanying the generation of photo-excited electrons (Path(1)). The reported potentials of the conduction and valence bands for ZnO NRs are -4.05 eV and -7.25 eV, respectively, and that of chemically reduced CNTs occurs around 4.7 – 4.8 eV [38–40]. The energies of these bands suggest that the excited electrons should directly transfer from the RhB dye^* to the graphene-like surfaces of CNTs, except in the ultraviolet region.

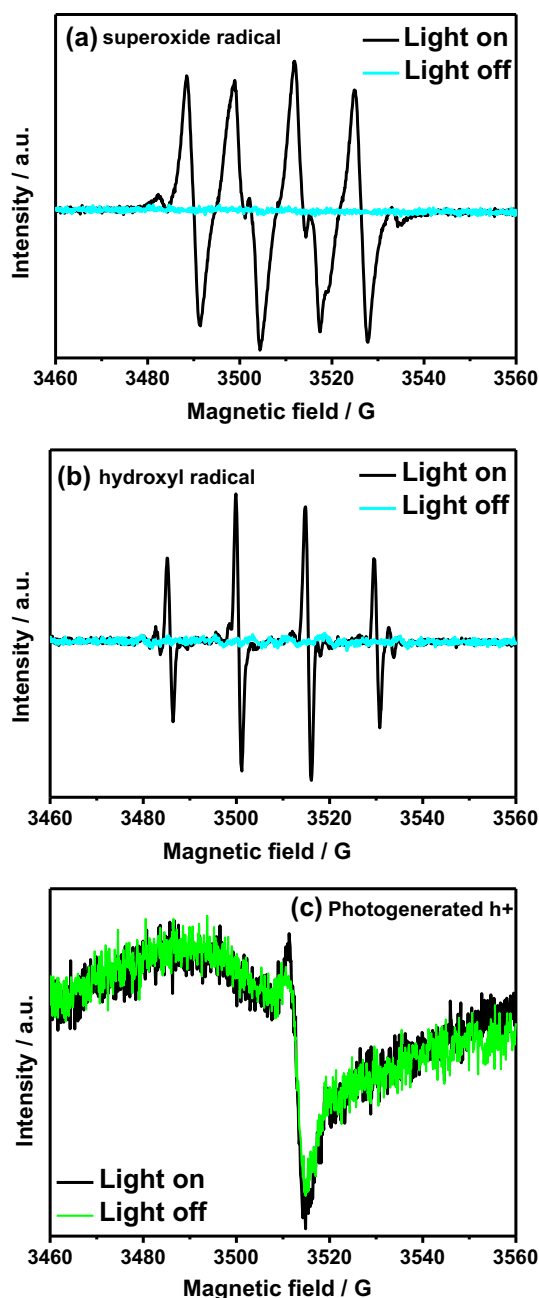


Fig. 11. Electron-spin-resonance spectra of $\text{ZnCT}_{\text{ethanol}}$ hybrid.

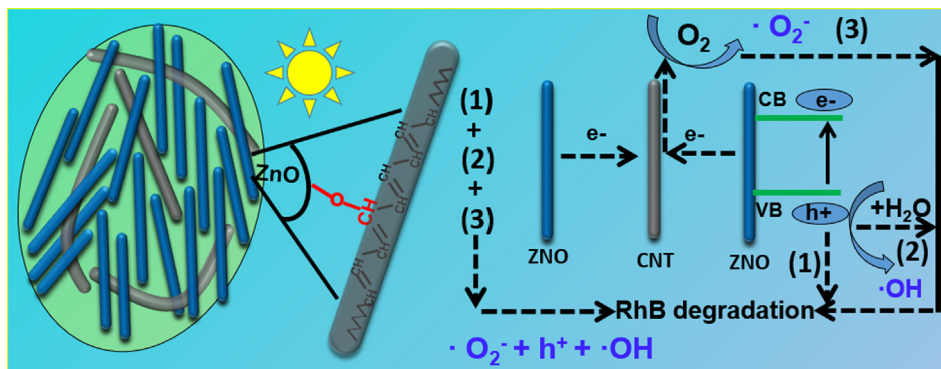


Fig. 12. Schematic diagram showing a proposed mixed oxidation pathway for RhB photodegradation by the ZnO/CNT hybrid. (1), (2) and (3) respectively represent the three paths to degrade RhB. (1) The holes naturally generated accompanying the generation of photogenerated electrons; (2) Hydroxyl radicals generated from the reaction of holes with H₂O; (3) Superoxide radicals generated from the reaction of electrons with the dissolved O₂.

The CNTs act as an effective and rapid electron acceptor due to the covalent Zn–O–C bonding between ZnO and CNTs during the *in-situ* synthetic process, helping lengthen the lifetime of the excited electrons derived from ZnO NRs, as confirmed by the TPV and photocurrents measurements performed in the absence of H₂O₂ [4,13,39]. The efficient separation of electrons and holes in this material allows the photogenerated holes sufficient time to react directly with dyes. Alternatively, the separated electrons on CNTs can react with the dissolved surface oxygen to generate ·O₂⁻ (Path(2)), or the separated holes can react with H₂O to generate ·OH⁻ (Path(3)) [11,37]. The resultant free radicals can further react with the nearby dye molecules to facilitate complete degradation. In this way, effective electron separation together with quick electron transfer are responsible for the enhanced photodecomposition performance of the ZnO/CNT hybrid under solar spectrum light.

4. Conclusion

We have *in-situ* synthesized an efficient off-white ZnO/CNT hybrid photocatalyst and applied it towards the photodecomposition of RhB dyes. The hybrid catalyst, comprised of ZnO NRs covalently linked to monodispersed CNTs, is synthesized in alcohol-alkali solution, free of catalytic assistance. A series of morphology and structural characterization studies including: SEM, XRD, Raman, XPS, and UV–vis spectroscopy, demonstrate that the as-prepared ZnO_{ethanol} NRs in the ZnO/CNT hybrid grow longer along the vertical radial (0001) surface and develop a closer contact with CNTs than is observed with ZnO_{methanol} NRs. The covalent attachment of the ZnO NRs with the monodispersed CNTs through Zn–O–C bonding is confirmed by XPS and Raman analysis of the ZnO/CNT hybrid. The light harvesting properties of this material are demonstrated via UV–vis measurements, which indicate high light absorption across the visible-ultraviolet light region. Probing the photocatalytic activity of the ZnO/CNT hybrid indicates the highest photocatalytic activity for this material than either pure ZnO_{ethanol} NRs or ZnO_{methanol} NRs or ZnO/CNT_{methanol} hybrid; nearly complete degradation of a solution of 2 × 10⁻² mg/mL RhB is observed following 2 h of irradiation in the presence of 0.2 mg/mL of the photocatalyst hybrid. Even upon recycling of the catalyst three times, the catalytic activity maintains a 90% degradation of RhB after 2 h. The recycling performance of the ZnO/CNT hybrid indicates high resistance to photocorrosion. Appendage of carbon nanotubes to ZnO NRs can extend the light absorption wavelength range and improve the electrical conductivity of ZnO NRs. *In-situ* reaction forms covalent bonding and close contact connections between ZnO_{ethanol} NRs and f-CNTs, which results in the predicted extension of the light absorption

wavelength range and electrical conductivity of the ZnO NRs and provide an efficient pathway for acceleration of electron transfer. TPV and photocurrent measurements for the ZnO/CNT hybrid validate the reduction of the photoelectron-hole pair recombination and lengthening of the lifetime of the photogenerated electrons transferred to CNTs from ZnO surface. The assembly of ZnO NRs covalently bonding with monodispersed CNTs yields an enhanced activity of the ZnO/CNT hybrid compared to ZnO and suggests viability of these hybrid materials for practical applications.

Acknowledgments

This research was supported by the National Nature Science Foundation of China (61605167 and 11804289), China, the Program for Innovative Research Team (in Science and Technology) in University of Henan Province (19IRTSTHN026), China, the Key Scientific Research Project of Universities and Colleges in Henan Province (17A430028), China, the Plan for Scientific Innovation Talent of Henan Province (174100510014), China, the Outstanding Young Backbone Teacher Funding Project of Xuchang University, China, and the Science and Technology Bureau of Xuchang, China.

References

- [1] M. Han, S.J. Zhu, S.Y. Lu, Y.B. Song, B. Yang, Recent advances in photocatalysis for environmental applications, *J. Environ. Chem. Engineer. Nano Today* 19 (2018) 201–218.
- [2] W.W. Tie, S.S. Bhattacharyya, Y.N. Wang, W.W. He, S.H. Lee, Facile *in-situ* synthesis of a zinc oxide crystals/few-layered graphene flake composite for enhanced photocatalytic performance, *J. Photochem. Photobiol. A: Chemistry* 348 (2017) 89–95.
- [3] Z.J. Zhang, T.T. Zheng, X.M. Li, J.Y. Xu, H.B. Zeng, Progress of Carbon Quantum Dots in Photocatalysis Applications, *Part. Part. Syst. Charact.* 33 (2016) 457–472.
- [4] J. Wang, R.S. Chen, Y. Xia, G.F. Wang, H.Y. Zhao, L. Xiang, S. Komarneni, Cost-effective large-scale synthesis of oxygen-defective ZnO photocatalyst with superior activities under UV and visible light, *Ceram. Int.* 43 (2017) 1870–1879.
- [5] F.-X. Xiao, J.W. Miao, H.B. Tao, S.-F. Hung, H.-Y. Wang, H.B. Yang, J.Z. Chen, R. Chen, B. Liu, One-dimensional hybrid nanostructures for heterogeneous photocatalysis and photoelectrocatalysis, *Small* 11 (18) (2015) 2115–2131.
- [6] W.W. Tie, S.S. Bhattacharyya, Y.G. Zhang, Z. Zheng, T.H. Lee, S.W. Lee, T.H. Kim, Y.H. Lee, S.H. Lee, Field-induced stretching and dynamic reorientation of functionalized multiwalled carbon nanotube aggregates in nematic liquid crystals, *Carbon* 96 (2016) 548–556.
- [7] R. Basu, Effect of carbon nanotubes on the field-induced nematic switching, *Appl. Phys. Lett.* 103 (2013) 241906.
- [8] A. McLaren, T. Valdes-Solis, G.Q. Li, S.C. Tsang, Shape and size effects of ZnO nanocrystals on photocatalytic activity, *J. Am. Chem. Soc.* 131 (2009) 12540–12541.
- [9] R.X. Shi, P. Yang, X.L. Song, J.P. Wang, Q.D. Che, A.Y. Zhang, ZnO flower: Self-assembly growth from nanosheets with exposed 1100 facet, white emission, and enhanced photocatalysis, *Applied Surface Science* 366 (2016) 506–513.

- [10] B. Cheng, E.T. Samulski, Hydrothermal synthesis of one-dimensional ZnO nanostructures with different aspect ratios, *Chem. Commun.* 8 (8) (2004) 986–987.
- [11] M.J. Sampaio, A. Benyounes, J.L. Faria, C.G. Silva, Photocatalytic synthesis of vanillin using N-doped carbon nanotubes/ZnO catalysts under UV-LED irradiation, *Applied Catalysis A: General*. 551 (2018) 71–78.
- [12] R.T. Thomas, R.P. Abdul, N. Sandhyarani, Synthesis of nanotitania decorated few-layer graphene for enhanced visible light driven photocatalysis, *J. Colloid Interf. Sci.* 428 (2014) 214–221.
- [13] J.B. Mu, C.L. Shao, Z.C. Guo, Z.Y. Zhang, M.Y. Zhang, P. Zhang, B. Chen, Y.C. Liu, High photocatalytic activity of ZnO-carbon nanofiber heteroarchitectures, *ACS Appl. Mater. Inter.* 3 (2011) 590–596.
- [14] F.T. Johra, W.G. Jung, RGO-TiO₂-ZnO composites: Synthesis, characterization, and application to photocatalysis, *Appl. Catal. A: Gen.* 491 (2015) 52–57.
- [15] C.S. Chen, T.G. Liu, L.W. Lin, X.D. Xie, X.H. Chen, Q.C. Liu, B. Liang, W.W. Yu, C.Y. Qiu, Multi-walled carbon nanotube-supported metal-doped ZnO nanoparticles and their photocatalytic property, *J. Nanopart. Res.* 15 (2013) 1295–1303.
- [16] S. Shoji, H. Suzuki, R.P. Zaccaria, Z. Sekkat, S. Kawata, Optical polarizer made of uniaxially aligned short single-wall carbon nanotubes embedded in a polymer film, *Phys. Rev. B* 77 (2008) 153407.
- [17] N. Ramesh Reddy, U. Bhargav, B. Chandra Mohan, M. Mamatha Kumari, M.V. Shankar, Multiwalled carbon nanotubes in titania based nanocomposite as trap for photoexcitons for enhanced photocatalytic hydrogen production under solar light irradiation, *Mater. Res. Bull.* 106 (2018) 271–275.
- [18] C.-I. Hung, H.-Ch. Wen, Y.-C. Lai, S.-H. Chang, W.-C. Chou, W.-K. Hsu, ZnO-Coated Carbon Nanotubes: Inter-diffusion of carboxyl groups and enhanced photocurrent generation, *Mater. Res. Bull.* 106 (2018) 271–275.
- [19] M. Samadi, H.A. Shivaee, M. Zanetti, A. Pourjavadi, A. Moshfegh, Visible light photocatalytic activity of novel MWCNT-doped ZnO electrospun nanofibers, *J. Mol. Catal. A* 359 (2012) 42–48.
- [20] Y. Bu, Z. Chen, W. Li, B. Hou, Highly efficient photocatalytic performance of graphene-ZnO quasi-shell-core composite material, *ACS Appl. Mater. Interfaces* 5 (2013) 12361–12368.
- [21] R. Beura, P. Thangadurai, Structural, optical and photocatalytic properties of graphene-ZnO nanocomposites for varied compositions, *J. Phys. Chem. Solids*. 102 (2017) 168–177.
- [22] R. Basu, D. Kinnamon, A. Garvey, Nano-electromechanical rotation of graphene and giant enhancement in dielectric anisotropy in a liquid crystal, *Appl. Phys. Lett.* 106 (2015) 201909.
- [23] W.W. Tie, S.S. Bhattacharyya, Y.H. Gao, Z. Zheng, E.J. Shin, T.H. Kim, M.S. Kim, J. H. Lee, S.H. Lee, Dynamic response of graphitic flakes in nematic liquid crystals: confinement and host effect, *Nanomaterials* 7 (2017) 250.
- [24] T.Z. Shen, S.H. Hong, J.K. Song, Electro-optical switching of graphene oxide liquid crystals with an extremely large Kerr coefficient, *Nature Mater.* 13 (2014) 394–399.
- [25] O. Yaroshchuk, S. Tomylo, O. Kovalchuk, N. Lebovka, Liquid crystal suspensions of carbon nanotubes assisted by organically modified Laponite nanoplatelets, *Carbon* 68 (2014) 389–398.
- [26] Y. Lei, L.Y. Gu, W.W. He, Z.X. Jia, X.G. Yang, H.M. Jia, Z. Zheng, Intrinsic charge carrier dynamics and device stability of perovskite/ZnO mesostructured solar cells in moisture, *J. Mater. Chem. A* 4 (2016) 5474–5481.
- [27] X.Q. Zhang, Y.Y. Feng, S.D. Tang, W. Feng, Preparation of a graphene oxide-phthalocyanine hybrid through strong p-p interactions, *Carbon* 48 (2010) 211–216.
- [28] D. Polsongkram, P. Chamninok, S. Pukird, L. Chow, O. Lupan, G. Chai, H. Khallaf, S. Park, A. Schulte, Effect of synthesis conditions on the growth of ZnO nanorods via hydrothermal method, *Physica B* 403 (2008) 3713–3717.
- [29] P.K. Giri, S. Bhattacharyya, D.K. Singh, R. Kesavamoorthy, B.K. Panigrahi, K.G.M. Nair, Correlation between microstructure and optical properties of ZnO nanoparticles synthesized by ball milling, *J. Appl. Phys.* 102 (2007) 093515.
- [30] J.F. Wang, T. Tsuzuki, B. Tang, X.L. Hou, L. Sun, X.G. Wang, Reduced graphene oxide/ZnO composite: reusable adsorbent for pollutant management. *Appl. Mater. Inter.* 4 (2012) 3084–3090. 28
- [31] M.-C. Hung, S.-Y. Yuan, C.-C. Hung, C.-L. Cheng, H.-C. Ho, T.-H. Ko, Effectiveness of ZnO/carbon-based material as a catalyst for photodegradation of acrolein, *Carbon* 66 (2014) 93–104.
- [32] F.C. Romeiro, M.A. Rodrigues, L.A.J. Silva, A.C. Catto, L.F. da Silva, E. Longo, E. Nossol, R.C. Lima, rGO-ZnO nanocomposites for high electrocatalytic effect on water oxidation obtained by microwave-hydrothermal method, *Appl. Surf. Sci.* 423 (2017) 743–751.
- [33] L.Q. Jing, B.Q. Wang, B.F. Xin, S.D. Li, K.Y. Shi, W.M. Cai, H.G. Fu, Investigations on the surface modification of ZnO nanoparticle photocatalyst by depositing Pd, *J. Solid State Chem.* 177 (2004) 4221–4227.
- [34] M.M. Hossain, B.-C. Ku, J.R. Hahn, Synthesis of an efficient white-light photocatalyst composite of graphene and ZnO nanoparticles: Application to methylene blue dye decomposition, *Appl. Surf. Sci.* 353 (2015) 55–65.
- [35] J. Wang, Z. Wang, B. Huang, Y. Ma, Y. Liu, X. Qin, X. Zhang, Y. Dai, Oxygen vacancy induced band-gap narrowing and enhanced visible light photocatalytic activity of ZnO, *ACS Appl. Mater. Interfaces* 4 (2012) 4024–4030.
- [36] N. Song, H.Q. Fan, H.L. Tian, Reduced graphene oxide/ZnO nanohybrids: Metallic Zn powder induced one-step synthesis for enhanced photocurrent and photocatalytic response, *Appl. Surf. Sci.* 353 (2015) 580–587.
- [37] M. Salavati-Niasari, F. Davara, M. Bazarganipour, Synthesis, characterization and catalytic oxidation of para-xylene by a manganese (III) Schiff base complex on functionalized multi-wall carbon nanotubes (MWNTs), *Dalton Trans.* 39 (2010) 7330–7337.
- [38] M. Samadi, H.A. Shivaee, M. Zanetti, A. Pourjavadi, A. Moshfegh, Visible light photocatalytic activity of novel MWCNT-doped ZnO electrospun nanofibers, *J. Mol. Catal. A* 359 42–48 (2012) 32.
- [39] B.J. Li, H.Q. Cao, ZnO@graphene composite with enhanced performance for the removal of dye from water, *J. Mater. Chem.* 21 (2011) 3346–3349.
- [40] I. Robel, B.A. Bunker, P.V. Kamat, Single-walled Carbon nanotube-CdS nanocomposites as light-harvesting assemblies: photoinduced charge-transfer interactions, *Adv. Mater.* 17 (2005) 2458–2463.